Original Article

Preparation and physical properties of conductive silk fabrics used in wearable clothes and flexible supercapacitors

M Khairy[1,2] $\textcircled{\tiny iD}$, R Kamal[1,3] and MA Mousa[1]

Abstract

The present work was designed to study several functions of Silk coated with polyaniline (PANI), graphene oxide (GO), and a composite of PANI@GO. The samples were characterized by XRD, SEM, FTIR, and thermal analysis. The investigated fabrics' resistivity, weight gain, tensile strength, elongation, and antimicrobial efficiency were monitored according to ASTM procedures. The FTIR spectra show the presence of the GO and PANI functional groups in the treated fabrics, and the SEM images show the formation of coating materials on the silk surface. The electrical conductivity of the coated silk with composite PANI@GO is 29 times higher than that of the uncoated one. The heat generation efficiency of the studied fabrics is in the order: of PANI@GO-SL > PANI-SL > GO-SL > SL. All coated silk samples have antimicrobial activity in the order: PANI@GO-SL > PANI-SL > GO-SL > SL. The results showed that the PANI@GO-SL sample exhibits the highest specific capacitance of all the coated silk electrodes with 450 Fg^{-1} at 10 mVs^{-1}, which renders PANI@GO-SL fabric a promising electrode material for supercapacitors. The capacitance value of the symmetric capacitor of PANI@GO-SL/PVA/ PANI@GO-SL using PVA-H_3PO_4 gel as an electrolyte is 71.2 Fg^{-1} at a current density of

[1]Chemistry Department, Benha University Faculty of Science, Benha, Egypt
[2]Chemistry Department, Imam Mohammad Ibn Saud Islamic University (IMSIU), Riyadh, Kingdom of Saudi Arabia
[3]Ministry of Trade and Industry (Industrial Control Authority), Egypt

Corresponding author:
M Khairy, Chemistry Department, Benha University Faculty of Science, faculty of science street, Benha13511, Egypt.
Email: mohkhairy@fsc.bu.edu.eg

one Ag^{-1} and 87.4% retention at 5000 cycles. The Ragone plot of the symmetric cell showed the highest energy density is 25.31 Wh/kg and a power density of 8018 W/kg. The results suggest using coated silk (PANI@GO-SL) prepared via low-cost processing as smart textiles for different applications.

Introduction

Textiles with multi functionalities are increasingly demanded as a part of advanced and future marketing strategies. Global trends are shifting towards environmentally friendly fabrics. Therefore, natural fiber applications are gaining traction globally that have expanded the use of silk fiber beyond the conventional textile industry due to their unique properties and functionality over synthetic fibers and their sustainability. Silk is a natural protein polymer with reactive functional groups, allowing them to be cross-linked with other polymers to be used in several applications. Coating and lamination are two operational processes that are used to make a proper finishing to the textile material. Textile coatings usually provide material layers that adhere to the textile structures and extend the range of their functional performance properties. Properties of coated textile materials primarily depend on their application. Modern technologies, optimization of the production process conditions, and the use of specific agents and recipes enable making a target product that will meet all the requirements. Since it is impossible to use the classic textile for many technical purposes, excellent properties are obtained by combining it with other substances coated in the form of paste or laminated to the material. Using value-added material, nano products, and modern technology can enhance the use of textile materials several times.[1–3] Several routes have been used to fabricate conductive textiles, such as creating metal fibers, coating the textile with metallic salts, and introducing intrinsically conductive polymers.[4,5]

Amongst these approaches, textiles coated with electrically conducting polymers are the most encouraging and simplistic methods for fabricating textile supercapacitors. Electric-heat conversion is a crucial way to be used in numerous applications such as heaters and thermoelectric power generators. Many thermal materials, such as conducting polymers, have been used for these applications. Polyaniline (PANI) is the most significant polymer due to its environmental stability, moderate conductivity, and diverse oxidation states. The in-situ chemical polymerization method is one of the various methods used for synthesizing polyaniline.[6] This method has some benefits over the other reported methods due to its eco-friendly, simplicity, and lower cost. The aniline monomer can be quickly deposited on the fabric surface.[6]

Due to graphene oxide's excellent dispersion and solubility, which contains many hydrophilic groups on its surface, it is easy to join with PANI.[7–9] Thus, PANI@GO composite material turns out to be an appropriate applicant for the manufacture of

functional fabrics by deposition and chemical polymerization methods. The considerable benefit of the presence of PANI in the composite is to increase the electrical conductance in the coated fabric.

Silk fabric is a highly water-absorbent material. Moreover, it is porous and lightweight. Therefore, the production of compressible silk supercapacitors integrated into clothes is worth investigating. The electrodes used for making supercapacitors should have a large area to provide appropriate energy.[10]

Little research has been registered about conducting fabrics' electrical properties, and there is a shortage in their electronic fields. Therefore, the present work was done to prepare conductive silk based on low-price abundant raw materials and simple preparation methods but tried to improve the performances of its electronic and thermal properties significantly. We have used PANI-Silk, GO-Silk, and PANI@GO-Silk fabrics via in-situ chemical oxidation polymerization and vacuum filtration. Several techniques characterized the control silk and the coated silk samples. Furthermore, we studied the treated silk's conductivity and thermal and electrochemical properties to test the possibility of using them as electrodes in supercapacitor devices. We also investigated the possibility of using the treated fabrics in UV protection and antimicrobial clothes.

Experimental

Materials

All chemicals are reagents used without further purification. Aniline, H_2SO_4 (98%), HNO_3 (32.5%), potassium permanganate ($KMnO_4$) (97%), sodium nitrate ($NaNO_3$) (95%), and sodium hydroxide (NaOH) (98.5%) delivered from ADWIC, HNO_3 (55%), and HCl (30%) supplied from DOP ORGANIK KIMYA SAN. VE TIC.LTD.STI, ammonium persulphate delivered from oxford (98%), graphite (99.995%) supplied from Fluka AG, and H_2O_2 (50%) provided from El Salam for chemical industries. The silk fabrics were purchased from the Egyptian market with a specification of warp and weft count: 23.3 dtex/2; warp density: 50 threads/cm; weft density: 45 threads/cm; and weight per unit area: 35 g/m^2.

Graphene oxide preparation

Modified Hummers-Offeman's method synthesized the graphene oxide (GO).[11,12] 5 g of graphite powder was placed in a flask. Then, 120 mL of H_2SO_4 was added by stirring in an ice-water bath, and 2.5 g $NaNO_3$ followed by 22.5 g of $KMnO_4$ was slowly added over about 2 h. The temperature of the reaction mixture should not exceed 20°C. After that, the flask was placed in an oil bath at 35°C for 2 h, and 250 mL of distilled water was added into the flask, which caused the temperature to increase to 95°C; after 1 h stirring, 50 mL of H_2O_2 was added, and the mixture was stirred for 2 h at room temperature. Finally, the mixture was centrifuged and washed with boiling distilled water until it became neutral. The resultant powder was dried at 60°C for 48 h to get the GO sample.

Preparation of GO-Silk fabric

First, the silk fabric was washed with 60°C deionized water to remove impurities before use. 10 mL of an ultrasonic dispersing aqueous solution of GO with a concentration of 5 mg mL^{-1} was poured onto the silk fabric fitted in the Buchner funnel of a suction flask (5 cm diameter) to fabricate the GO/silk material. After filtration, the composites were removed from the funnel and air-dried. The produced fabric showed black color and symbolized GO-SL.

Preparation of PANI-Silk coated fabrics

Silk fabrics were cut into a circle diameter of 2.5 cm and cleaned before the coating using ethyl alcohol for 30 min in an ultrasonic bath; after that, washed them with distilled water before drying in an oven at 45°C. The silk fabrics were coated with PANI via the precipitation method. This was done by oxidation of aniline dissolved in 1M nitric acid solution (0.2 M) in the presence of fabrics by 0.2 M solution of $(NH_4)_2S_2O_8$ under vigorously stirring under ultrasonication for 1 h. Finally, the fabrics were left overnight in the reaction mixture, washed with distilled water, and dried in an oven for half an hour at 60°C. After coating with polyaniline, the produced fabrics had dark green and symbolized PANI-SL.

Preparation of PANI@GO-Silk fabric

The prepared GO-Silk fabric sample was immersed in a beaker containing 80 mL anhydrous ethyl alcohol, nitric acid, and 20 mL aniline monomer for 90 min. Ammonium persulfate in a molar ratio with aniline and HNO$_3$ of 1: 1: 0.5 was added gradually to the above solution. The polymerization procedure was carried out at 20°C for another 120 min to get silk fabric coated with dark green nanocomposites, symbolized as PANI@GO-SL.

Characterization

The untreated and treated silk fabrics were dried at 40°C for 24 h and kept in a desiccator before making any measurements. XRD analysis was carried out by a Diano (U.S.A.). The patterns were measured with CuKα radiation (λ = 1.5418 Å). The diffractograms were recorded at *2θ* angles between 5 and 70°. The SEM images were taken using the scanning electron microscope (Philips SEM 515), where the accelerating voltage was kept at 3 kV. Prior to imaging, all the samples were coated with Leica EM ACE600 gold coater (Leica Microsystems Pty Ltd., Macquarie Park, NSW, Australia). An infrared spectrophotometer (Perkin-Elmer Model 883) was employed to record the ATR FT-IR spectra in the range of 4000-400 cm^{-1}. The thermal stability of the silk and the PANI@GO-silk fabrics was measured by the TG/DTA instrument of Shimadzu model TGA-50H. In the experiment, argon was used as the carrier gas with a flow rate of 50 mL min^{-1}, and the heating rate was controlled at 10°C min^{-1}. Fabric tensile strength test was conducted

according to ASTM method 1682 (1994) using an Electronic Universal Testing Machine (UTM), Instron 3369, at 30°C with a tensile speed of 0.009 mm/s. The fabric width and length were 50 mm and 200 mm respectively. Each sample was repeated five times. The UV- protection efficiency of the coated fabrics is analyzed at a wavelength between 280-400 nm. The mean UPF values were evaluated based on the Australian/New Zealand Standard (AS/NZS 4399:1996 Sun protective clothing–evaluation and classification, Standards Australia, Sydney). The heat generation capacity of the examined conducting fabric was measured using a 9 V battery as a power source connected to a square ship of the fabric (6 cm × 6 cm). The obtained current was measured using an electrometer model 6517, Keithley, and the temperature was determined using an Omega infrared thermometer sited in the middle of the sample. All the determinations of the heat generation were done in triplicate, and the results present mean values.

Electrical properties

The electrical properties were measured at a constant voltage (1 V), in a frequency range between 10^3 and 10^6 Hz at 25°C, using a programmable automatic LCR bridge (HIOKI: 3532–50). The a.c. Conductivity (σ_{ac}) is obtained from the data of dielectric constant (ε') and loss tan δ using the relation $\sigma_{ac} = \varepsilon' \varepsilon_o \omega$ tan δ, where ε_o is the permittivity of vacuum and ω is the angular frequency. The ε'−values are calculated using the relation $\varepsilon' = (C/\varepsilon_o)$ x(t/A), where C is the equivalent capacitance, t is the thickness of the sample, A is the area of the specimen, tan δ is the dissipative factor. The bulk dc-conductivity σ_{dc} of the material was measured using an electrical circuit consisting of a voltameter (Keithley, 2182), an electrometer (model 6517, Keithley), and a 5 V dc power supply. The bulk dc-conductivity σ_{dc} of the material was estimated utilizing the equation: $\sigma_{dc} = (t/A) \times (1/R_{dc})$; where R_{dc} is the resistance of the sample. The Surface resistance was also determined on the fabric sample (6 cm^2) using the four-probe method, which indicates the ratio of the voltage drop between one pair of electrodes with current flow between the other pair of electrodes placed opposite each other in the case of square-shaped samples. The measurements were made using a combination of a low current DC source Keithley 6220 precision current source and a high resistance electrometer – Keithley 6517 electrometer. To measure the surface resistance, a small current ranging from 1 μA to 1 mA was passed through the sample, and the voltage drop was measured with the voltameter (Keithley, 2182). The surface electrical conductivity is evaluated using the relation: $\sigma_s = (I/\Delta V) \times (t/A)$; where ΔV is the measured voltage drop, I is the current passed through the sample. Each of the conductivity results is the observation of five repetitions, and the measurement error is estimated using the standard deviation formula. Electrochemical measurements were performed with an SP 300, BioLogic potentiostat by performing galvanostatic charge/discharge (GCD), cyclic voltammetry (CV), and electrochemical impedance spectroscopy (EIS) analyses.

Electrochemical Properties

Aqueous Supercapacitor. The silk electrode's electrical capacitance was investigated by employing a three-electrode cell containing the saturated calomel electrode (SCE) as a reference electrode and the platinum sheet with a surface area of 2 cm^2 as a counter electrode. The working electrodes were made up of pieces of fabrics where their upper edges were placed between two titanium plates to hang down with high stability in the electrolyte solution. The titanium plates were put to be not contacted with the electrolyte. The electrolyte used was a 1 M Na_2SO_4 solution. The experiments were done under a nitrogen atmosphere to remove oxygen from the solution.

Flexible solid-state supercapacitors fabrication. A solid-state symmetric supercapacitor was fabricated using a Swagelok cell with two PANI@GO-SL electrodes of the same mass and PVA-H_3PO_4 gel electrolytes. The two identical PANI@GO-SL electrodes were immersed in the H_3PO_4/PVA gel electrolyte for 10 min, then cured at room temperature over 4 h. The two electrodes were then tightly pressed for 10 min to allow the polymer gel electrolyte on each electrode to combine into one thin separating layer to form an integrated device. One cm-diameter disk was punched out of the fabric device and placed inside the Swagelok type two-electrode cells with stainless steel 316 current collectors. The PVA-H_3PO_4 gel electrolyte was prepared: 1 g of PVA was dispersed in 10 mL of double distilled water with stirring at 90°C to form a clear homogeneous solution. Next, 0.02 mol of H_3PO_4 was added to the solution with continuous stirring at room temperature for 24 h.

Antimicrobial Activity test

The silk fabric's antimicrobial activity n reducing microbe growth was determined according to AATCC Test Method 100–2004. The tested micro-organisms are *Escherichia coli (E. coli)*, *S. aureus*, and *Candida Albicans*. The initial micro-organism concentration used was about 10^5 CFU ml^{-1} for all experiments. The percentage reduction in the colony (R%) between the untreated and treated silks was determined after incubation for 24 h at 37°C by using the equation: R% = (B – A)/ B × 100, where B and A are the numbers of CFU ml^{-1} of micro-organisms determined for the untreated and the treated fabrics respectively.

Statistical analysis

All the quantitative data were expressed as a mean ± standard deviation (SD). The statistical analysis was carried out using one-way ANOVA, and a value of $p < 0.05$ was considered to be statistically significant.
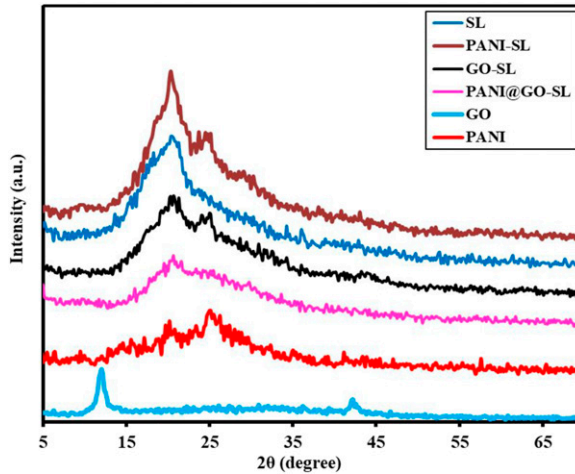
Figure 1. XRD patterns of the investigated fabrics.

Results and Discussion

XRD

XRD patterns of the coating materials (PANI, GO), raw silk (SL), and coated fabrics (PANI-SL, GO-SL, and PANI@GO-SL) are represented in Figure 1. The diffraction pattern of GO reveals a sharp peak at $2\theta = 12.01°$, attributed to the inter-planar spacing of GO sheets, and another peak at 42.3°, attributed to incomplete oxidation of graphite.[13] The X-ray diffraction of PANI shows mainly two peaks at $2\theta = 20.3°$ and 24.9°, corresponding to (020) and (200) crystal planes of PANI related to the periodicity parallel and perpendicular of PANI chains, respectively.[14] The diffraction patterns of raw silk fabric show a prominent peak at $2\theta = 20.5°$, which is attributed to the exceptionally ordered β-structure of silk.[15] However, the XRD patterns of the treated silk fabrics with PANI, GO, and PANI@GO (composites), given in Figure (1), show the same characteristic peaks of the coating material with a slight shift in their positions, besides a significant difference in the diffraction peak of the silk observed at 20.5°. It was also observed that the intensity of the peak appearing at 24.48° in PANI was decreased in the PANI@GO-SL. This may be attributed to decreasing the fabric's crystallinity as a result of some interactions of GO and PANI with the peptide linkages in the structure of silk fabrics.[16]

SEM

SEM analysis was done to confirm the presence of the coating materials on the Silk's surface. The results obtained are shown in Figure 2. The SEM image of the raw silk fabric shows a smooth and uniform appearance (Figure 2(a)), whereas the photograph of the GO-SL sample (Figure 2(b)) shows some aggregation of GO particles on the silk's
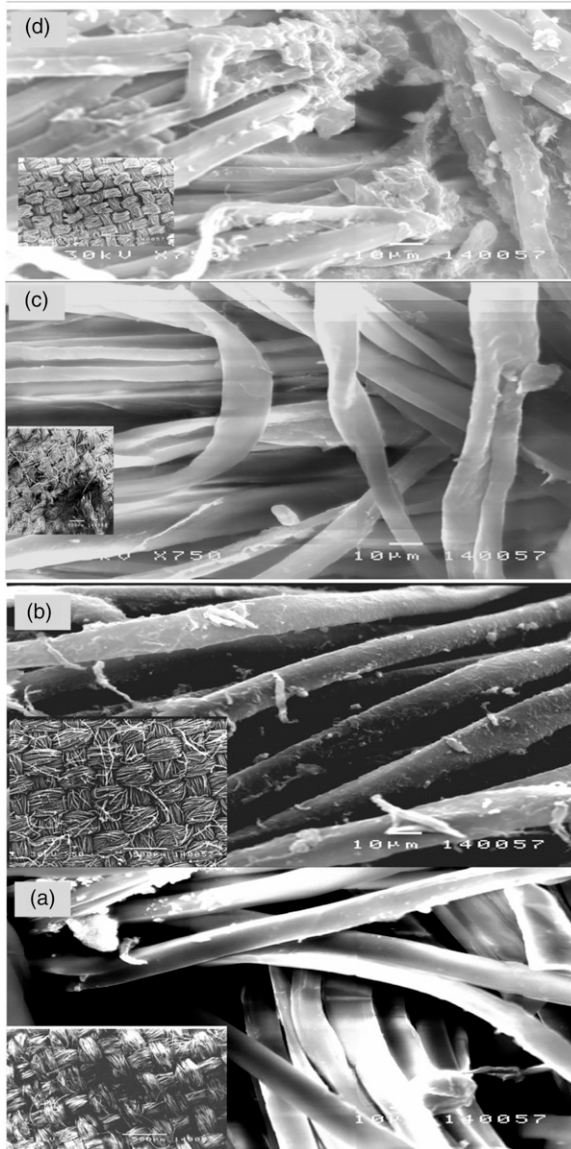
Figure 2. SEM image of (a) SL (b) PANI –SL (c) GO-SL (d) PANI@GO-SI.

surface. The micrograph of the silk fabrics coated with PANI (Figure 2(c)) shows an almost uniform surface covered with PANI sheets. On the other hand, the SEM image of PANI@GO-silk (Figure 2(d)) shows silk fibers coated with aggregated composite material. These results agree with XRD and FTIR results and elucidate the introduction of the
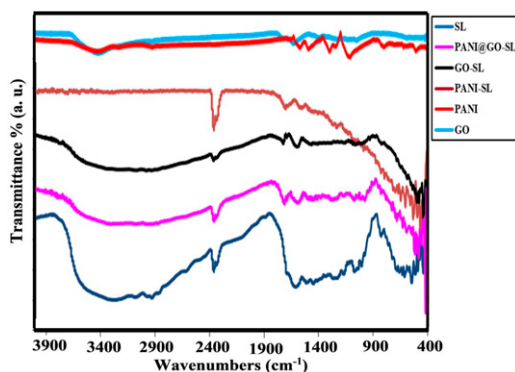
Figure 3. FTIR spectra of the investigated fabrics.

coating materials in Silk fabric. The SEM image of PANI@GO-silk (Figure 2(d)) shows regular and uniform morphology with some aggregation. These results agree with XRD and FTIR results and elucidate the introduction of the coating materials in Silk fabric.[17]

FTIR spectra analysis

The FTIR spectra of the studied fabrics are recorded in 4000–400 cm^{-1} and illustrated in Figure 3. The spectrum of control silk fabric reveals the prominent peak's vibrational modes: C=O at 1726 cm^{-1}, N—H stretching at 1611 cm^{-1}, C-N stretching at 1251 cm^{-1}, and -CH$_3$ stretching at 1446 cm^{-1}. The FTIR spectra of coating materials (PANI and GO) powders were performed to assign the discrete impacts of these materials, which might be seen in the spectra of coated fabrics. The existence of various categories of oxygen functionalities in GO was approved by the presence of a band at 3300 cm^{-1} that can be ascribed to the O-H stretching vibrations of the C-OH groups and H$_2$O,[18,19] a band at 1600 cm^{-1} (skeletal vibrations from unoxidized graphitic domains),[20] and band at 1050 cm^{-1} (C-O stretching vibrations).[21] However, the FT-IR spectrum of the polyaniline sample demonstrates its most essential characteristic bands at 1488 cm^{-1} and 1570 cm^{-1}, referring to C-N vibration of the benzenoid N–B–N and quinoid N=Q=N rings[22] (where B denotes the benzoic-type rings and Q represents to the quinolinic-type rings). These peaks approve of the formation of PANI. The peak detected at 1140 cm^{-1} is associated with the doped PANI chain with H$^+$.[23] The peak observed at 1100 cm^{-1} is a distinguishing for PANI conductance and the extent of the electron delocalization and is assigned to the vibration of C- H.[22] The band at 1295 cm^{-1} is agreed to the displacement of π electrons stimulated polymer by doping it by acid.[24] The spectrum of GO-silk shows bands at 1465 cm^{-1} due to C-OH stretching mode and C-C stretching mode at 1598 cm^{-1} and peaks at 1723 cm^{-1}, 1690 cm^{-1} corresponding to C=O (RCOOH). Moreover, absorption peaks observed for PANI-Silk at 817 cm^{-1}, 1170 cm^{-1}, 1300 cm^{-1}, and 1490 cm^{-1} are credited to the vibration of the C-H plane, C-N in PANI, and the aromatic C=C stretching
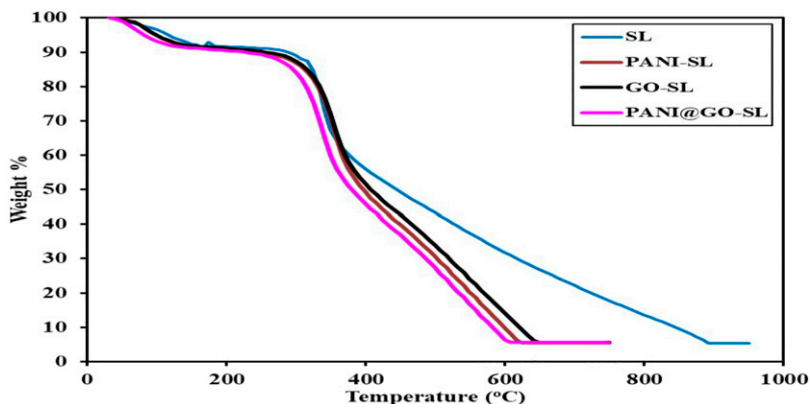
Figure 4. TGA thermograms of the investigated uncoated and coated silk.

vibration of the benzenoid ring, respectively. The change in the position and intensity of the absorption bands of untreated silk, shown in Figure 3, ensure that the silk fabric is coated by GO nanosheet and PANI. The coating materials seem to mask the fibroin band at 965 cm^{-1} characterized of −gly−gly− and −gly−ala− peptide backbone motifs.[25]

Thermal analysis

Thermal gravimetric analyses (TGA) were used to study the thermal stability of the silk (SL) and treated silk. The thermograms obtained are given in Figure 4. It shows that the thermal degradations for each sample occur mainly in several stages. The lower steps (at temperatures less than 250°C) are attributed to the loss of adsorption water and dopants and found to be 8.2, 8.4, 8.7, 9.1, and 9.5% for SL, SL-GO, SL-PANI, and PANI@GO-SL samples, respectively. The TGA steps observed at higher temperatures (more than ~250 $^{\circ}$) are ascribed to the degradation of the fabrics. The second stage appeared at a temperature range of 300–380°C showing a weight loss of 44.5.47.1, 47.9, and 49% are ascribed to starting the degradation of the silk proteins (sericin and fibroin) skeletal, PANI, and GO chains for SL, GO-SL PANI-SL, and PANI@GO-SL samples, respectively. The third step is attributed to the complete degradation of the samples. The TGA - results show that the thermal stability decreases in the order: SL > GO-SL > PAN-SL, and PANI@GO-SL. The decrease in the thermal stability of the silk fabric after its coating with GO and PANI refers to some interactions occurring between the coating materials and the silk causing weakness in the bonds of the fabric.[26] The results also show that the weight loss of coated fabrics is faster than that of untreated ones. From the remaining char, it is found that the percent of the undegradable part of the samples is 5.4, 5.45, 5.55, and 5.6% for SL, PANI-SL, GO-PANI, and PANI@GO-SL, respectively.

Table 1. Tensile strength and antimicrobial data of the investigated fabrics.

Sample	Tensile strength (N)	Elongation %	Antimicrobial reduction %		
			E. coli	S. aureus	Cand. Albicans
SL	251 ± 5.2 (259 ± 6.1)	6.5 ± 0.3 (6.6 ± 0.2)	14 ± 1	12 ± 1	10 ± 1
GO-SL	255 ± 4.3 (264 ± 4.7)	8.1 ± 0.4 (8.4 ± 0.4)	84 ± 2	85 ± 1	89 ± 2
PANI-SL	266 ± 4.5 (273 ± 5.1)	8.7 ± 0.2 (9.1 ± 0.2)	89 ± 2	76 ± 2	92 ± 2
PANI@GO-SL	273 ± 4.8 (281 ± 4.6)	9.2 ± 0.2 (9.5± 0.2)	97 ± 3	93 ± 2	98 ± 2

Wrap value ( ).

Mechanical properties

The tensile strength and elongation of the investigated fabrics were also measured and the results obtained are given in Table 1. The table shows that the mechanical properties of the coated silks increased significantly in the warp and weft directions compared with un-coated fabric. The presence of COOH, C=O, and NH_3^+ groups in GO and PANI coating materials could justify a better construction between nano/micro phase interfaces to provide better contact with the silk substrate, causing the coating materials' reinforcement effect. Increased tensile strength would be beneficial for applying silk fabric to decorative materials.

Laundering durability

The apparel fabrics application is greatly affected by the coating resistance to washing. The change in the weight after repetitive washing of the fabric samples was measured and given in Table 2 and Figure S1, which shows that the weight of all coated samples within the first three washing cycles is slightly decreased, except for the GO-SL sample; after that, the weight became constant. The PANI@GO-SL sample showed the lowest weight loss after 10 washing cycles. This indicates that these fabrics have good fastness to washing.

Heat Generation from Fabrics

One of the possible applications of the made coated silk fabrics, especially those exhibit high conductivity, is their use in heating devices. A setup, shown in Figure 5 (insert), was operated to measure the heat-generating capacity of the studied conducting silk. A 9 V battery as a power supply was connected to a square shape fabric (7 cm × 7 cm). The increase in temperature was recorded employing an Omega infrared thermometer located at the midpoint of the fabric. The change in temperature with time is illustrated in Figure 5. The results showed that a conventional 9-V battery could be used to warm the silk fabric treated with the different coated materials, and the heat generated decreases in the order: PANI@GO-SL > PANI-SL > GO-SL > SL. The current drawn in this experiment is very

Table 2. Weight changes of the investigated fabrics before and after washing.

Sample	Before washing Wt (gm)	After 1st washing Wt (gm)	After 2nd washing Wt (gm)	After 3rd washing Wt (gm)	After 5th washing4 Wt (gm)	After 10th washing Wt (gm)
SL	0.0144	0.0136	0.0135	0.0133	0.0131	0.0131
PANI-SL	0.0173	0.0164	0.0154	0.0152	0.0149	0.0149
GO-SL	0.0202	0.0181	0.0176	0.0175	0.0174	0.0174
PANI@ GO-SL	0.0165	0.0156	0.0154	0.0152	0.0147	0.0147
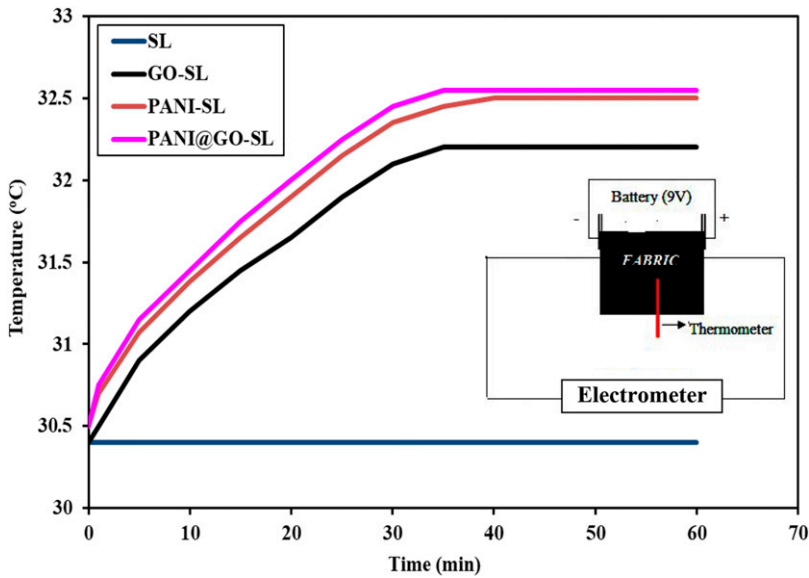
Figure 5. Heat-generation behavior of the investigated fabrics under voltage of 9V. The inset figure is the setup of the heating circuit.

low. Thus, the lifespan of a battery will be high, and an on/off switching unit within the person's clothing can utilize the power carefully as per needs.

UV radiation protection

To our knowledge, there are no studies on UV radiation protection for silk fabric coated with GO and PANI. The ultraviolet protection factor (UPF) for all the investigated samples was determined at a wavelength between 280-400 nm and found to be 37.1 ± 0.4, 44.3 ± 0.5, and 48.5 ± 0.4 for GO-Sl, PANI-SL, and PANI@GO-SL, respectively. They

are higher than that of silk fabric (UPF rating at 4.6). The results indicate that the composite layer of PANI@GO on the silk surface causes a more reduction in the transmittance of ultraviolet light than that of other individual coating materials.

Antimicrobial activity

The Gram-negative *Escherichia coli* (*E. coli*), Gram-positive *Staphylococcus aureus* (*S. aureus*), and Fungi *Candida Albicans* are used to test the antimicrobial activity of the investigated fabrics using AATCC Test Method 100–2004. The acquired results are given in Table 1, which shows that all coated silk samples have antimicrobial activity decreases in the order: PANI@GO-SL > PANI-SL > GO-SL > SL. It is thought that the electrostatic attraction between the negatively microbial cell and positively charged nanomaterials (such as PANI in our study) is an essential parameter for their antimicrobial activity.[27] The antimicrobial mechanism of GO is explained based on the fact that GO can destroy the microbial membranes, leading to the efflux of intracellular material and killing microbes.[28,29] It can also be said that the hydroxyl groups in GO interfere with microbial metabolism by piling at the cell surface and attaching with DNA to hinder m-RNA synthesis .[29, 30] The difference observed in the antimicrobial efficiency values can also be attributed to the dissimilarities in the structures of the microorganisms.

Electrical properties

dc Conductivity. The electrical conductivity properties of the studied fabrics were also investigated. I–V plots of the uncoated and coated silk in a voltage ranging between −10 to +10 V show linear I–V relations for all the coated silk samples. The bulk (σ_{dc}) and surface dc-conductivity ($\sigma_{dc/Su}$) of all the investigated samples, before and after the sample. The obtained results are shown in Figure 6 and Table 3, which show that σ_{dc} values of the coated samples are higher than that of the uncoated sample. The initiation of
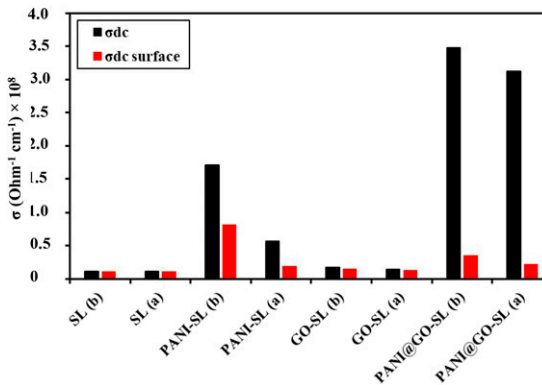

Figure 6. The surface and bulk conductivity of the investigated fabrics after washing (a) and before washing (b).

Table 3. Dc- and ac-electrical conductivity of the uncoated and coated Silk after 10 washing cycles.

Sample	$\sigma_{dc} \times 10^9$ $(Ohm^{-1}\ cm^{-1})$	σ_{dc} surface $\times 10^9$ $(Ohm^{-1}\ cm^{-1})$	$\sigma_{AC} \times 10^7$ at 1 MHz $(Ohm^{-1}\ cm^{-1})$
SL	1.10 (1.10) ± 0.02	1.11 (1.11) ± 0.02	0.5 ± 0.03
PANI-SL	5.71 (17.1) ± 0.05	1.94 (8.2) ± 0.02	300 ± 0.02
GO-SL	1.41 (1.72) ± 0.03	1.29 (1.51) ± 0.02	103 ± 0.02
PANI@GO-SL	31.27 (34.81) ± 0.12	2.21 (3.51) ± 0.01	150 ± 0.02

( ) after washing.

conductivity within silk matrix fabric is attributed to the diffusion of PANI and GO inside the fabrics and their coating on the silk surface to form a conducting path in the fabric. It can be said that the observed enhancement in conductivity could be attributed to two supplies, namely microscopic and macroscopic conductivities which are participating in the improvement conduction process.[31] The microscopic conductivity hangs on several factors, such as conjugation and chain length. On the contrary, the macroscopic conductivity is dependent on external factors such as molecular orientation. The conjugated structure of PANI chains with high conductivity and high surface area is also considered the main reason for increasing the conductivity of the treated fabric containing PANI. The PANI coated on the silk surface is emeraldine salt form as electrical conduction state. The monomer repeat unit of the doped form of the PANI comprises benzenoid (B) and quinoid (or quinonoid, Q) structures. Absorption bands ascribed to C–N stretching vibration in QBB structure (v_{QBB}) and BBQ structure (v_{BBQ}) are observed at 1295 cm^{-1}.[24] A mixed sequence is formed by the combination of Q and B structures. Polarons, the PANI's charge carriers, conduct electricity by moving along the main chain with the Q–B combination. Moreover, the distinguished surface area of the GO nanosheet helps to improve the homogeneous dispersion of polyaniline on the silk surface. Thus, it is deduced that the deposition of GO nanosheets onto the silk fabric develops the electrical conductance in PANI@GO-SL, as shown in our results.

ac Conductivity. The ac-electrical conductivity (σ_{ac}), at a frequency range of 10^3–10^7 Hz, was investigated to get information on the polarization in the coated silk. The σ_{ac} - value was evaluated using equation (1)[32]

$$\sigma_{ac} = \varepsilon' \varepsilon_o \omega \tan \delta \qquad (1)$$

where V_r is the applied potential, ϕ is the phase angle, and R is the resistance used.

The frequency dependence of the ac-conductivity of SL, PANI-SL, GO-SL, and PANI@GO-SL is given in Figure S2. It shows that the electrical conductivity value (σ_{ac}), at each measuring frequency decreases in the order: PANI-SL > PANI@GO-SL > GO-SL >SL

We can attribute the lower conductivity values of the samples containing GO compared with that of other coated pieces to the lower electrical conductivity value of GO than

PANI; besides, it can make barrier ways to prevent the moving of electrons in the PANI@ GO-SL sample. The lower conductivity values of the samples containing GO compared with that of other coated pieces may be attributed to GO's lower electrical conductivity value than PANI; besides, it can make barrier ways prevent the moving of electrons in the PANI@GO-SL sample. Figure S2 also shows that as the frequency increases, the ac-conductivity increases. This is because the frequency acts as a pushing force for charges and facilitates the polarization processes.

Electrochemical Study

The capacitance behavior of the uncoated and coated silk electrodes was studied using cyclic voltammetry (CV) and galvanostatic charge-discharge (GCD). Figure 7 depicts the CV curves for the investigated electrode samples at a scan rate of 10 mVs^{-1}. It is evident from the Figure that the silk electrode sample shows a rectangular shape that refers to a double-layer capacitance. In contrast, the coated silk electrodes containing the PANI, GO, and GO/PANI composites electrodes exhibit two pairs of redox peaks representing their pseudocapacitive characteristics. The redox peaks of the samples containing PANI are attributed to the redox transition of PANI from a semiconducting state (leucoemeraldine form) to a conducting state (polaronic emeraldine form) and faradaic transformation between the emeraldine and pernigraniline states .[33] The specific capacitance values C_{sp} were calculated from CV plots using the following equation [34]

$$C_{sp} = \int I(V)dV \bigg/ (2mv\Delta V)$$ (2)

where m is the mass of the active electrode material, v is the scan rate, ΔV is the potential window, and $\int I(V)dV$ is the integrated area of the CV curves. The specific capacitances
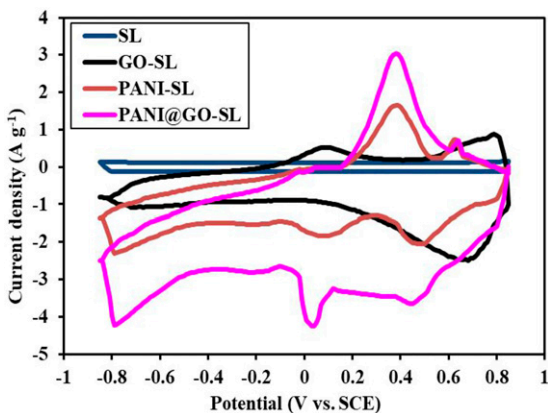

Figure 7. Cyclic Voltammetry of the undoped and doped silk at 10 mV/s in 1 M Na$_2$SO$_4$.

calculated using equation (3) were found to be 6.5, 231, 332, 450 Fg^{-1} for SL, GO-SL, PANI-SL, and PANI@GO-SL electrodes at a scan rate of 10 mVs^{-1} in 1 M Na$_2$SO$_4$.

The highest capacitance of the binary composite electrode, PANI@GO-SL, is attributed to a synergetic effect of the individual component in the composite material and the contribution of double-layer capacitance with the pseudocapacitance. The composite electrode exhibits numerous distinctive characteristics causing it to be an encouraging applicant for high-performance electrode materials. These properties involve: (a) the porous structure of the textile permitted uniform coating of GO and the following loading of PANI. Accordingly, it simplified the connection of electrolyte ions to the electrode surface. (b) Across in-situ electrochemical polymerization, a good interface contact between PANI and GO can be produced to realize rapid electron transfer. (c) PANI guaranteed high pseudocapacitive capacitance and a small path ion diffusion throughout the charge-discharge procedure. Since the PANI@GO-SL electrode exhibits the highest capacitance of all studied coated electrodes; therefore, it was further characterized under different scan rates. Figure 8 shows the CV curves of PANI@GO-SL at the scan rates from 1 to 50 mV s^{-1}. As the scan rate increases, the oxidation and reduction peaks shift to higher and lower potentials. Since the area within a CV curve is directly proportional to its specific capacitance, therefore, it can be seen that the specific capacitance decreases as the scan rate increases. This could be attached to the large ohmic resistance at the high scan rate. Besides, the electrolyte ions do not have enough time, at high scan rates, to fully diffuse through the electrode nanopores wherever the faradaic reactions occur.

Using PVA/H$_3$PO$_4$ gel as a solid electrolyte, two PANI@GO-SL (highest capacitance of all the electrodes) electrodes were collected into a solid-state symmetric supercapacitor. Figure 8(a) demonstrates the CV curves of the supercapacitor at different scan rates. The figure shows high capacitance rising from the high conductivity of GO and the large pseudocapacitance of PANI. The capacitance increases with increasing scan rates. The device supplies capacitance values of 74, 72, 70.5, 69.4, 68.1, and 66.9 Fg^{-1} at scan rates of 1, 2.5, 5, 10, 20, and 50 mVs^{-1}.

The galvanostatic charge-discharge (GCD) behavior of the symmetric solid capacitors was also studied using different current densities. The obtained results are shown in Figure 8(b). The departure in the linearity of the discharge plots can be attributed to the pseudocapacitance mechanism resulting from the faradic process.

The cell capacitance (C_{cell}) values were calculated from the galvanostatic discharge curves using equation (3).[35]

$$C_{cell} = I*\Delta t / M*\Delta V \qquad (3)$$

Where I is the constant discharge current, ΔV is the working voltage, Δt is the discharging time, and M is the total mass of the active materials on two electrodes. The results obtained are 71.2, 70.1, 68.5, 66.8, and 66.4 F/g at 1, 3, 5, 8, and 10 A/g, respectively, which agree well with those obtained from CV measurements.

The cyclic stability of the symmetric cell was also tested by GCD measurement for 5000 cycles at a current density of one Ag^{-1} (Figure 8(c)). The capacitance remained
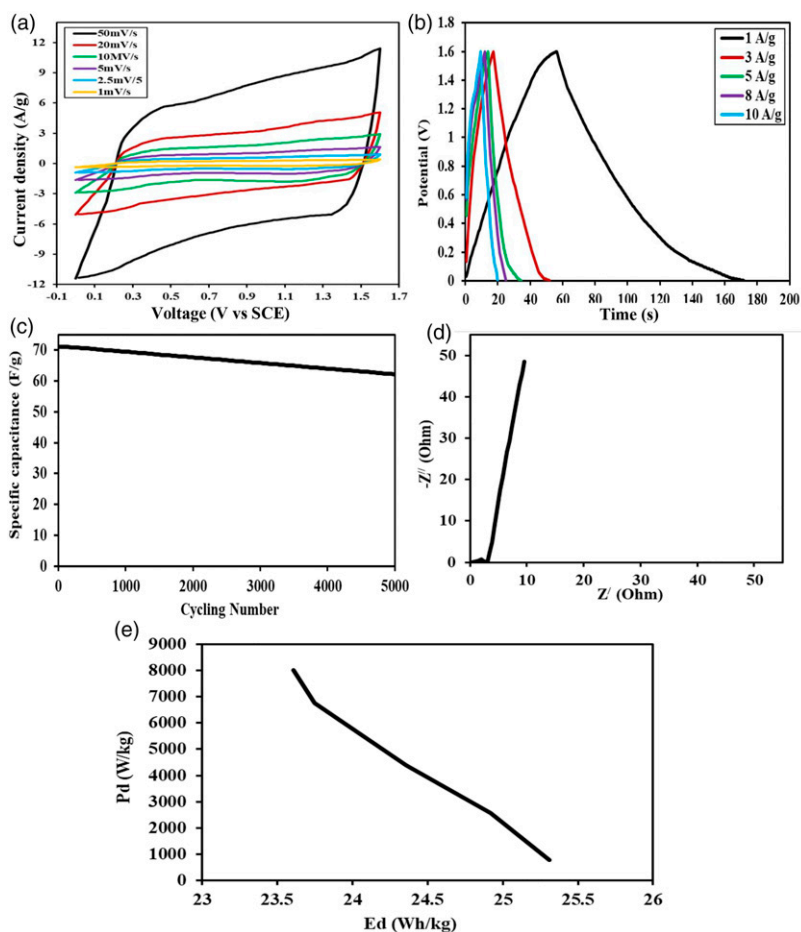
Figure 8. Electrochemical properties of symmetric cell PANI@GO-SL// PANI@GO-SL (a) Cyclic Voltamogram at different scan rates, (b) GCD at different current densities, (c) Stability of the symmetric cell during 5000 cycles, (d) Nyquist plots and (e) Ragone plot.

87.4% after 5000 cycles. The gradual decrease of capacitance was possibly attributed to drying the gel electrolyte.

Figure 8(d) demonstrates the Nyquist plot of the symmetric PANI@GO-SL super-capacitor. The figure shows a semicircle in the high-frequency region. The intersection point between the semicircle and the Z''- axis is about 0.38 Ω, representing a low equivalent series resistance (ESR). The semicircle diameter represents the charge-transfer resistance (R_{ct}) produced from the Faradic reaction, and electrochemical double-layer capacitance is found to be 2.7 Ω. The fast rise at the nearly vertical line at the low-frequency region is due to the capacitive behavior. From the maximum frequency ($f°$, Hz) at Z'' on the semicircle in the impedance spectrum, the time constant (τ, s) of the

Table 4. A comparison between electrochemical data of some supercapacitors found in literature and the data of the present work.

Material	Electrolyte	E_d (Wh kg^{-1})	P_d (W kg^{-1})	Cs_P Fg^{-1}	Ref
CNPCF/PPY SC cell	1 M LiClO$_4$	38.9	—	280.4 at 0.42 mAcm^{-2}	[36]
CNPCF SC	1 M LiClO$_4$	—		31.4	[36]
CNPs/UCF	—	30	32,000	154	[37]
MAF-rGO	1 M Li$_2$SO$_4$	—		142 at 1 Ag^{-1}	[38]
HCNTF SC	5 M KOH	16.3	—	125.7	[39]
HHC9K4	6 M KOH	3.53	325	999 at 1 Ag^{-1}	[40]
AC from tremella	6 M KOH	9.6	124	71 at 1 Ag^{-1}	[41]
OCNTF-PPY-50	1 M LiClO$_4$	42	—	305	[42]
Co-rGO/silk fibroin	EMIm$^+$BF$_4^-$	28.31	78.24	104 at 0.5 A g^{-1}	[43]
PANI@GO-SL// PVA	PVA-H$_3$PO$_4$ gel	25.31	8018	72.1 at 1 A/g	This work
PANI@GO-SL	1 M Na$_2$SO$_4$	—		450 at 10 mVs^{-1}	

symmetric capacitor is determined using the equation: $\tau = 1/f$ [35] and is found to be 7.2 ms. The small-time constant reveals the high power response of the device. The specific energy density and power density of the symmetric PANI@GO-SL supercapacitor device are calculated by equations (4) and (5),[34] respectively

$$E_d = C_{ell}(\Delta V)^2/7.2 \tag{4}$$

$$P_d = 3600*E_d/t \tag{5}$$

Where ΔV is the operating voltage and t is the discharging time. The energy densities of the symmetric cell at various power densities (Ragon plots) are shown in Figure 8(e). The symmetric cell exhibits a maximum energy density of 25.31 Wh/kg and a maximum power density of 8018 W/kg. The electrochemical data obtained in the present study and other similar systems found in the literature[36–43] are listed in Table 4, which shows that our symmetric capacitor exhibit higher energy and power density than many other systems.

Conclusions

The coating is a powerful tool for the advancement of textile technology. It provides the opportunities to produce unique fabrics for Medical applications, heat-sensitive fabrics, automotive fabrics, disposable hospital apparel, etc. The present study reports a superficial and eco-friendly methodology for preparing coated silk fabrics by GO, PANI, and PANI@GO nanocomposite. The silk surfaces of the raw and treated fabrics have been characterized using XRD, ATR-FTIR, SEM, and TGA The mechanical properties,

dc-, ac-electrical conductivity, electrochemical properties, and antimicrobial tests were also studied. The FT-IR spectra approved the functional groups of the investigated samples, while XRD spectra reveal that the investigated coating material and fabrics possess amorphous structures. SEM studies showed that the coating materials were deposited on the treated fabric surface. Comparing the electrical conductivity values of the raw and treated fabrics refers to the penetration of coating materials inside the fabrics. The treated fabrics showed high UV protection, an improvement in the fabric's tensile properties, and antimicrobial efficiency against *Escherichia coli* (*E. coli*), *S. aureus*, and *Candida Albicans in the order:* PANI@GO-SL > PANI-SL > GO-SL > SL. The electrical capacitance of the uncoated and coated silk in 1 M Na_2SO_4 showed an increase in the specific capacitance in the same order observed for antimicrobial efficiency. Symmetric solid supercapacitor using PANI@GO-SL electrodes and H_3PO_4/PVA gel showed a specific capacitance of 71.2 F/g at a current density of 1 A/g. The symmetric cell exhibits a maximum energy density of 25.31 kWh/kg and a maximum power density of 8018 W/kg. The obtained results are significant because they may allow using coated fabrics in industrial applications. Generally, the treated silk fabrics improved electrical conductivity, UV-protection ability, antibacterial activity, and other physical properties—including tensile properties. Therefore, it can be said that the investigated coated silk with multifunctional properties has high potential in the textile industry.

Declaration of conflicting interests

Funding

ORCID iD

M Khairy https://orcid.org/0000-0002-6343-5250

Supplemental Material

Supplemental material for this article is available online.

References

1. Ashish KS. *Coated Textiles Principles and Applications*. 2nd edn. CRC Press, 2007.
2. Sukanta P, Sourav M, Ajit D, et al. Multifunctional textile fabric and their application. *J Fashion Technol Textile Eng* 2021; 9: 6.
3. Islam GMN. Applications of Nanotechnology in Textiles: A Review. *Adv Res Text Eng* 2019; 4: 1038.
4. Gokarnesha N and Srivatsav GN. Some Significant Trends in Conductive Textiles. *Latest Trends Textile Fash Des* 2018; 2(3): 179–186.

5. Tang XN, Tian MW, Qu LJ, et al. Functionalization of cotton fabric with graphene oxide nanosheet and polyaniline for conductive and UV blocking properties. *Synth Met* 2015; 202: 82–88.
6. Ameen S, Akhtar MS and Husain M. A review on synthesis processing chemical and conduction properties of polyaniline v and its nanocomposites. *Sci Adv Mater* 2010; 2: 441–446.
7. Wang L, Lu X, Lei Sh-B, et al. Graphene-based polyaniline nanocomposites: Preparation, properties and applications. *J Mater Chem A* 2014; 2: 4491–4509.
8. Huang Z, Li L, Wang Y, et al. Polyaniline/graphene nanocomposites towards high-performance supercapacitors: A review. *Compos Commun* 2018; 8: 83–91.
9. Chauhan S. Graphene Oxide/Polyaniline Composites as Electrode Material for Supercapacitors. *J Chem Pharm Res* 2017; 9: 285–291.
10. Gonçalves AG, Jarrais B, Pereira C, et al. Functionalization of textiles with multi-walled carbon nanotubes by a novel dyeing-like process. *J Mater Sci* 2012; 13: 5263–5275.
11. Hummers WS and Offerman RE. Preparation of Graphitic Oxide. *J Am Chem Soc* 1958; 80: 1339–1339.
12. Cote LJ, Kim F and Huang J. Langmuir−Blodgett Assembly of Graphite Oxide Single Layers. *J Am Chem Soc* 2009; 131: 1043–1049.
13. Dong LM, Wua KJ, Shi DY, et al. Graphene quantum dots with its amino-functionalization prepared by the microwave-hydrothermal method. *Dig J Nanomater Bios* 2015; 10: 1215–1227.
14. Abdiryim T, Xiao-Gang Z and Jamal R. Comparative studies of solid-state synthesized polyaniline doped with inorganic acids. *Mater Chem Phys* 2005; 90: 367–372.
15. Manickam P and Thilagavathi G. A natural fungal extract for improving dyeability and antibacterial activity of silk fabric. *J Ind Text* 2015; 44: 769–780.
16. Xia YY and Lu Y. Fabrication and properties of conductive conjugated polymers/silk fibroin composite fibers. *Compos Sci Technol* 2008; 68: 1471–1479.
17. Cao J and Wanga C. Highly conductive and flexible silk fabric via electrostatic self assemble between reduced graphene oxide and polyaniline. *Org Electron* 2018; 55: 26–34.
18. Padmavathy N and Vijayaraghavan R. Enhanced bioactivity of ZnO nanoparticles - an antimicrobial study. *Sci Technol Adv Mat* 2008; 9: 35004–35010.
19. Zhang T, Zhang D and Shen M. Low-cost method for preliminary separation of reduced graphene oxide nanosheets. *Mater Lett* 2009; 63: 2051–2054.
20. Si Y and Samulski ET. Synthesis of water soluble graphene. *Nano Lett* 2008; 8: 1679–1682.
21. Xu Y, Bai H, Lu G, et al. Flexible graphene films via the filtration of water-soluble noncovalent functionalized graphene sheets. *J Am Chem Soc* 2008; 130: 5856–5857.
22. Tan Q, Xu Y, Yang J, et al. Preparation and electrochemical properties of the ternary nanocomposite of polyaniline/activated carbon/TiO_2 nanowires for supercapacitors. *Electrochim Acta* 2013; 88: 526–529.
23. Łużny W, Śniechowski M and Laska J. Structural properties of emeraldine base and the role of water contents: X-ray diffraction and computer modeling study. *Synth Met* 2002; 126: 27–35.
24. Gomes EC and Oliveira MAS. Chemical Polymerization of Aniline in Hydrochloric Acid (HCl) and Formic Acid (HCOOH) Media. Differences between the Two Synthesized Polyanilines. *Am J Polym Sci* 2012; 2: 5–13.

25. Arai T, Freddi G, Innocenti R, et al. Biodegradation of Bombyx mori silk fibroin fibers and films. *J Appl Polym Sci* 2004; 91: 2383–2390.

26. Rosa IM, Kenny JM, Puglia D, et al. Morphological, thermal and mechanical characterization of okra (Abelmoschus esculentus) fibres as potential reinforcement in polymer composites. *Compos Sci Technol* 2010; 70: 116–122.

27. Macasaquit AC and Bing CA. Preparation of conducting polyester textile by in situ polymerizations of pyrrole. *Philipp J Sci* 2010; 139: 189–196.

28. Hiba M, Ajay K, Elena B, et al. Antimicrobial mechanisms and effectiveness of graphene and graphene-functionalized biomaterials. a scope review. *Front Bioeng Biotechnol* 2020; 8: 465.

29. Purwar R and Joshi M. Recent developments in antimicrobial finishing of textiles-a review. *AATCC Rev* 2004; 4: 22–26.

30. Tu Y, Lv M, Xiu P, et al. Destructive extraction of phospholipids from *Escherichia coli* membranes by graphene nanosheets. *Nat Nanotechnol* 2013; 8: 594–601.

31. Sudha, Nair SS and Kumar D. Investigations on Functioning of Conducting Fabrics for Application in Wearable Clothes. *IJRAT* 2014; 2: 77–84.

32. Pervaiz E E. and Gul IH. Enhancement of Electrical Properties Due to Cr^{+3} Substitution in Co-Ferrite Nano Particles Synthesized by Two Chemical Techniques. *J Magn Magn Mater* 2012; 324: 3695–3703.

33. Wang YG, Li HQ and Xia YY. Ordered Whiskerlike Polyaniline Grown on the Surface of Mesoporous Carbon and Its Electrochemical Capacitance Performance. *Adv Mater* 2006; 18: 2619–2623.

34. Isacfranklin M, Yuvakkumar R, Ravi G, et al. Quaternary Cu_2FeSnS_4/PVP/rGO Composite for Supercapacitor Applications. *ACS Omega* 2021; 6: 9471–9481.

35. El-Shahat M, Mochtar M, Rashad MM, et al. Single and ternary nanocomposite electrodes of Mn_3O_4/TiO_2/rGO for supercapacitors. *J Solid State Electrochem* 2021; 25: 803–819.

36. Jayesh C and Kar KK. Hierarchical carbon nanopetal/polypyrrole nanocomposite electrodes with brush-like architecture for supercapacitors. *Phys Chem Chem Phys* 2016; 18: 8587–8597.

37. Cherusseri J and Kar KK. Hierarchically mesoporous carbon nanopetals based electrodes for flexible supercapacitors with super-long cyclic stability. *J Mater Chem A* 2015; 3: 21586–21598.

38. Yaswanth KP, Prerna S, Amit KY, et al. Al^{3+}-doped 3d-transitional metal (Mn/Cu) ferrite impregnated rGO for PEC water-splitting/supercapacitor electrode with oxygen vacancies and surface intercalation aspects. *Composites B* 2020; 202: 108431.

39. Jayesh C, Raghunandan S and Kar KK. Helically coiled carbon nanotube electrodes for flexible supercapacitors. *Carbon* 2016; 105: 113–125.

40. Prerna S, Amit Y, Alekha T, et al. Keratin-derived functional carbon with superior charge storage and transport for high-performance supercapacitors. *Carbon* 2020; 168: 419–438.

41. Guo N, Li M, Sun X, et al. Tremella derived ultrahigh specific surface area activated carbon for high performance supercapacitor. *Mater Chem Phys* 2017; 201: 399–407.

42. Cherusseri J and Kar KK. Ultra-flexible fibrous supercapacitor with carbon nanotube/polypyrrole brush-like electrodes. *J Mater Chem A* 2016; 4: 9910–9922.

43. Tanmoy R, Nilkamal P and Sandeep K. High electrochemical performance flexible solid-state supercapacitor based on Co-doped reduced graphene oxide and silk fibroin composites. *Energy* 2017; 141: 1982–1988.